Cation/anion-based electrochemical degradation and rejuvenation of electrochromic nickel oxide thin films

*Hui-Ying Qu [a,b], Daniel Primetzhofer [c], Zhen Qiu [a], Lars Österlund [a], Claes G. Granqvist [a], and Gunnar A. Niklasson *[a]*

[a] Dr. Hui-Ying Qu, Dr. Zhen Qiu, Prof. Lars Österlund, Prof. Claes G. Granqvist [a], Prof. Gunnar A. Niklasson, Department of Engineering Sciences, The Ångström Laboratory, Uppsala University, SE-75121 Uppsala, Sweden

[b] Dr. Hui-Ying Qu, MIIT Key Laboratory of Critical Materials Technology for New Energy Conversion and Storage, School of Chemistry and Chemical Engineering, Harbin Institute of Technology, 150001 Harbin, China

[c] Prof. Daniel Primetzhofer, Department of Physics and Astronomy, The Ångström Laboratory, Uppsala University, SE-75120 Uppsala, Sweden

Ni oxide thin films are widely used in electrochromic (EC) devices with variable throughput of visible light and solar energy. However, the mechanisms underlying the optical modulation—and its degradation under extended operation and subsequent rejuvenation—are poorly understood especially for Li^+-conducting electrolytes. Here we report on a comprehensive study of the EC properties of sputter-deposited Ni oxide films immersed in an electrolyte of $LiClO_4$ in propylene carbonate. Cyclic voltammetry and optical transmittance measurements were used to document degradation and subsequent potentiostatic rejuvenation. X-ray diffraction did not show evidence for accompanying changes in crystallinity, whereas vibrational spectroscopy indicated that degraded films had carbonaceous surface layers. Time-of-flight elastic recoil detection analysis demonstrated that both Li^+ ions and Cl-based ions participate in the electrochromism and its degradation and rejuvenation. A major result was that degradation is associated with a reduced difference in the concentrations of Li^+ and Cl-based ions in the nickel oxide during extended electrochemical cycling, and rejuvenation of degraded films is achieved by removal of Li^+ ions and accumulation of Cl-based anions so as to regain their initial concentration difference. Our work provides new insights into the use of ion-exchange-based devices incorporating nickel oxide.

KEYWORDS: Electrochromism, nickel oxide film, degradation, rejuvenation, ToF-ERDA

……..

*Corresponding author: gunnar.niklasson@angstrom.uu.se

1. Introduction

New sustainable technology is needed to meet growing global demands for energy, and electrochromics can play an important role in this context.[1] An electrochromic (EC) device is able to regulate its transmittance of visible light and solar energy,[2–4] and thin-film devices can be utilized for automatic as well as operator-based control of glazing in buildings which combine energy efficiency, due to lower need for air conditioning, with good indoor comfort.[5] Not surprisingly there is large and growing interest in EC materials and associated device technology.

Electrochromism is a common phenomenon, and recent studies have dealt with transition metal oxides and with various types of organic materials.[6–9] However, it appears that only the oxides are currently used in glazing, which may be due to their documented ruggedness under practical operation. As for any ion-exchange-based construction, it is inevitable that oxide-based EC materials degrade in performance upon long-term electrochemical cycling, and numerous studies to improve the durability have been carried out and have used doping elements,[10–13] nanostructural modification,[14–16] and hybrid materials (including inorganic–inorganic and inorganic–organic hybrids).[17,18] However the requirement that EC-based glazing withstands electrochemical cycling between states of high and low transmittance during a lifetime exceeding 20 years remains challenging. A recent discovery demonstrated a new approach to tackle degradation and pave the way towards long-term use of EC devices. It was unambiguously demonstrated that several kinds of degraded cathodic EC films—including oxides of W, Ti and Mo—could be rejuvenated and regain their original properties by electrochemical posttreatment.[19–23] These investigations, as well as subsequent characterization studies,[24,25] firmly showed that degradation of these EC oxides is related to Li^+ ion trapping and that the same oxides can be rejuvenated by electrochemically induced extraction of trapped Li^+ ions.

The oxides mentioned above color cathodically, *i.e.*, under ion insertion, and another type of EC oxides color anodically, *i.e.*, under ion extraction, with Ni oxide being the most prominent example.[26–28] Combinations of W-oxide-based and Ni-oxide-based thin films are employed in most of today's EC glazing.[3,29] Films of Ni oxide are also subject to significant degradation upon electrochemical cycling,[30–33] and many uncertainties pertain to the durability of Ni-oxide-based EC films: thus it is not fully clear what ionic species are involved

in the electrochromism, especially in the case of Li^+-based electrolytes,[34–36] and the physical and chemical origins of the irreversibility as well as the coloration mechanism are uncertain, experimentally as well as theoretically. However, it is commonly accepted that cations (Li^+ ions in the case of lithium-based electrolytes) participate in the electrochromism of Ni oxide and that its optical properties are modulated by reversible charge-transfer processes between Ni^{2+} and Ni^{3+}.[37] Recent work of ours[38] demonstrated that Ni-oxide-based films can be rejuvenated and showed that both Li^+ ions and Cl-based ions participate in this process. In the present comprehensive paper we present more detailed information on EC coloration, degradation and rejuvenation in Ni-oxide-based films, as studied with a range of characterization techniques. In particular, we show that the *difference* in concentration between Li^+ ions and Cl-based ions plays a decisive role for the electrochromism.

2. Results and Discussion

2.1 Electrochromic and Electrochemical Data

Ni oxide films were prepared by sputter deposition onto glass substrates coated with electrically conducting transparent layers of In_2O_3:Sn (known as ITO) as further discussed in the experimental section below. Figure 1 reports electrochemical and electrochromic data for a Ni oxide film immersed in an electrolyte of $LiClO_4$ in propylene carbonate (PC) and subjected to various treatments. Cyclic voltammetry (CV) measurements (Figure 1b) were carried out in a conventional operating range of 2.0–4.0 V at a scanning rate of 50 mV s^{-1} and commenced from an open-circuit potential (OCP) of ~3.3 V. Significant changes of the voltammograms occurred during 500 cycles, and the charge capacity—governed by the encircled area during consecutive voltage sweeps in the positive and negative directions—exhibits a pronounced decrease. The associated mid-luminous optical modulation range drops significantly (Figure 1a); the degradation is most prominent for the colored state, while the bleached-state transmittance remains almost unchanged, as shown in detail from spectral transmittance data (Figure 1c) taken in the luminous wavelength range. Importantly, we found that, except for the first CV cycle, the charge capacity during coloration was larger than that during bleaching (Figure 1d). This observation is significant for understanding the coloration mechanism of Ni oxide, which becomes optically absorbing as a result of the extraction of positive ions (and/or insertion of negative ions). During the first CV cycle it seemed that an excess of positive ions was inserted into the film, but during subsequent cycles it was not

straightforward to distinguish the possible contributions of positive and negative charges. The excess charge density during the initial bleaching was 0.27 mC cm^{-2}, which is much less than the accumulated excess charge density for coloration during subsequent CV cycles (115 mC cm^{-2}). Obviously, any Li^+ ions participating in the electrochromism cannot be extracted to a larger extent than they are inserted, which would be the case if nothing but Li^+ ions took part in the coloration and bleaching processes.

Rejuvenation of degraded electrochromism was investigated by performing potentiostatic experiments, specifically sequentially applying potentials of 4.1 and 1.6 V. As shown in Figure 1a, the optical transmittance of the degraded film decreased to 65% during the application of 4.1 V for 20 h, which is somewhat lower than the initial colored-state transmittance. Subsequent to this treatment, the Ni oxide film was "rested" at zero potential for 2 h in order to reach a stable state, at which the OCP was ~3.7 V. It is apparent that the initial colored-state transmittance was almost recovered when CV cycling was resumed after the resting period (Figure 1a), and the rejuvenated Ni oxide film displayed virtually the same EC properties as the as-deposited film in the entire visible wavelength range during the first CV cycle after rejuvenation (Figure 1c). Furthermore, the EC properties evolved during 500 subsequent CV cycles in essentially the same manner as during the first 500 cycles. Figure 1e shows current density evolution during rejuvenation and exhibits a rapid initial drop followed by a constant or slowly decreasing value during most of the process. This residual current density may be dominated by parasitic side reactions in the electrolyte.

Next, we applied a constant potential of 1.6 V to the Ni-oxide-based film. The optical transmittance remained high and unaltered as long as this potential was applied and also during a following 2-h resting period. This property is the expected one since the bleached state in Ni oxide is attained at low potentials. The optical transmittance modulation after applying 1.6 V showed that the colored state had recovered somewhat but was still far from its initial transmittance (Figure 1a, c), and a final round of 500 CV cycles yielded rather constant optical modulation. The charge capacity after two CV cycles was only slightly larger than that of the film degraded after 500 cycles, but the CV data were not comparable with those after rejuvenation at 4.1 V (Figure 1b). Hence the electrochromism had recovered somewhat, but full rejuvenation was not accomplished.

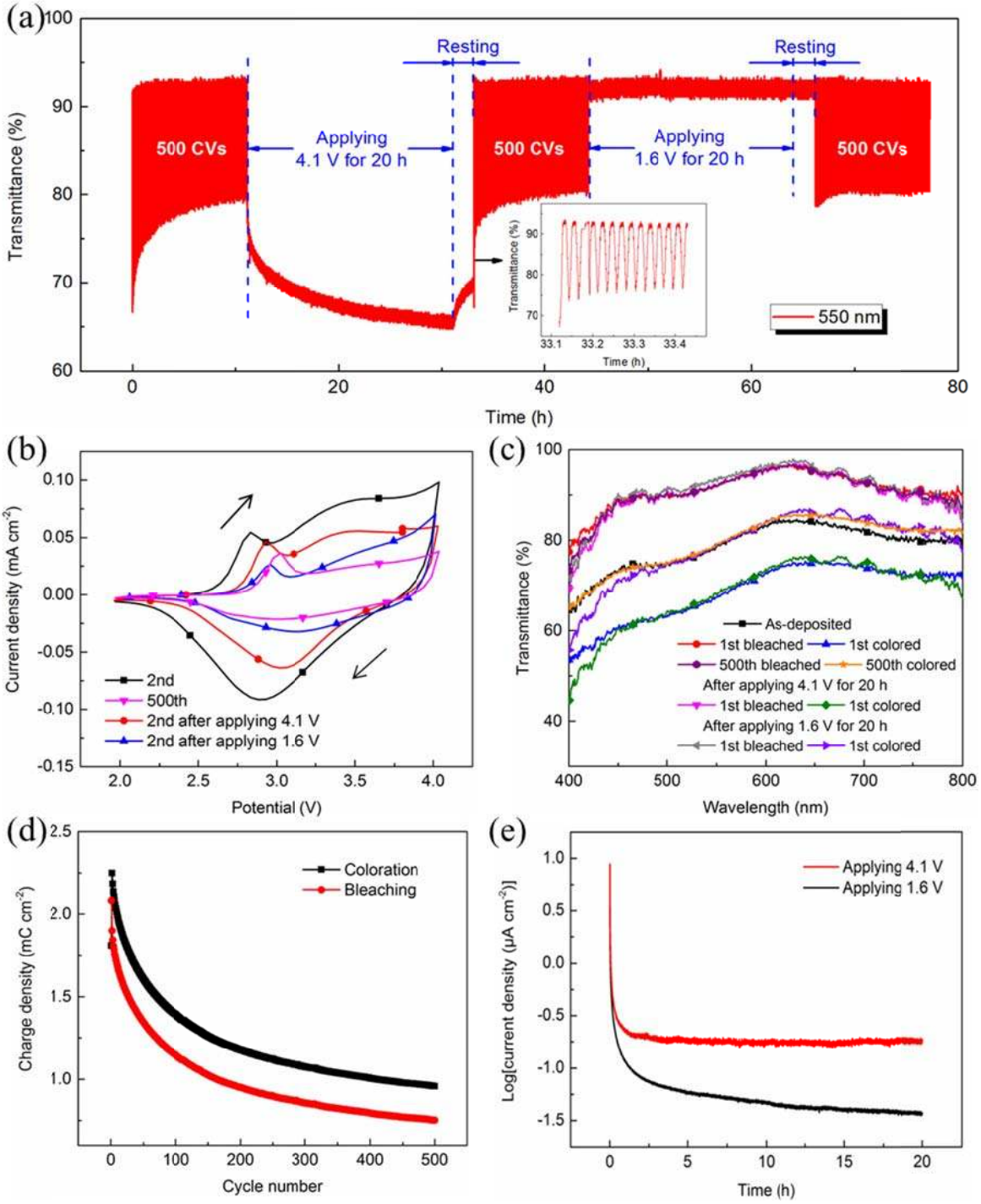

Figure 1. Electrochemical and electrochromic performance of a ~300-nm-thick Ni oxide film subjected to varied operations. (a) Optical transmittance at a wavelength of 550 nm during voltammetric cycling in the range of 2.0–4.0 V *vs*. Li/Li^+, at a scan speed of 50 mV s^{-1}, before and after potentiostatic treatments at the indicated voltages; inset gives a time-resolved rendition of the transmittance during the initial voltage cycles after applying 4.1 V *vs*. Li/Li^+ followed by a 2-h resting period. (b) Cyclic voltammograms for the indicated cycles recorded at 50 mV s^{-1}; arrows indicate scan direction. (c) Spectral optical transmittance for the film in as-deposited state, after bleaching and coloring for the indicated cycles, and subsequent to the shown potentiostatic treatments; some curves are overlapping. (d) Charge density during coloration and bleaching *vs*. cycle number for an as-deposited film. (e) Logarithm of current density *vs*. time during potentiostatic treatments at the shown voltages.

It is important to elucidate whether rejuvenation can occur spontaneously in the absence of an applied voltage, *i.e.*, while keeping the film at the OCP. To that end, as illustrated in Figure 2, we subjected a Ni oxide film to 500 CV cycles as before, followed by a 20-h waiting period, and a subsequent second round of 500 CV cycles. Clearly, neither the optical data (Figure 2a, c) nor the cyclic voltammograms (Figure 2b) were influenced to any significant degree by the waiting period. However, rejuvenation by applying 4.1 V for 20 h, followed by a resting period, essentially brought back the EC properties of the as-deposited film, which agrees with the results in Figure 1.

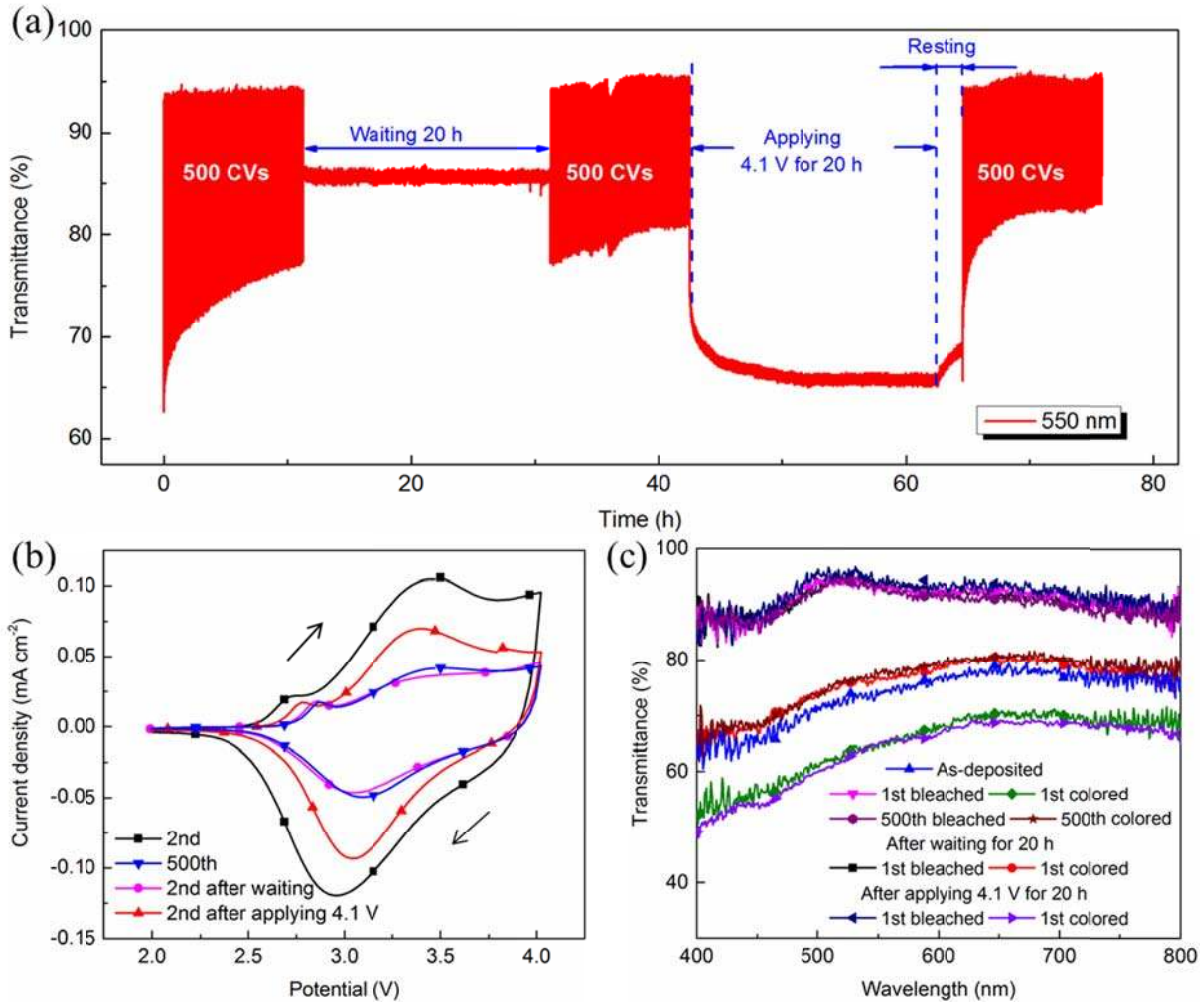

Figure 2. Electrochemical and electrochromic performance of a ~300-nm-thick Ni oxide film subjected to varied operations. (a) Optical transmittance at a wavelength of 550 nm during voltammetric cycling in the range of 2.0–4.0 V *vs*. Li/Li$^+$, at a scan speed of 50 mV s^{-1}, before and after the indicated treatments. (b) Cyclic voltammograms for the indicated cycles recorded at 50 mV s^{-1}; arrows denote scan direction. (c) Spectral optical transmittance for the film in as-deposited state, after bleaching and coloring for the indicated cycles, and subsequent to the shown treatments; some curves are overlapping.

2.2 Characterization by X-ray Diffraction and Vibrational Spectroscopy

Several characterization techniques were used in order to shed light on the species involved in the coloration, degradation and rejuvenation of the Ni-oxide-based film on ITO-coated glass. Figure 3a shows X-ray diffraction (XRD) patterns for samples in as-deposited state, after 500 CV cycles as described above, and after rejuvenation by applying 4.1 V for 20 h. All films were found to be crystalline, and the Ni oxide had a face-centered cubic (fcc) NiO structure (Joint Commission of Powder Diffraction Standards, JCDPS No. 47-1049) with clear diffraction peaks from the (111), (200), (220), (311) and (222) lattice planes. No significant difference could be associated with degradation and rejuvenation. Diffraction peaks from ITO were well separated from those due to NiO.

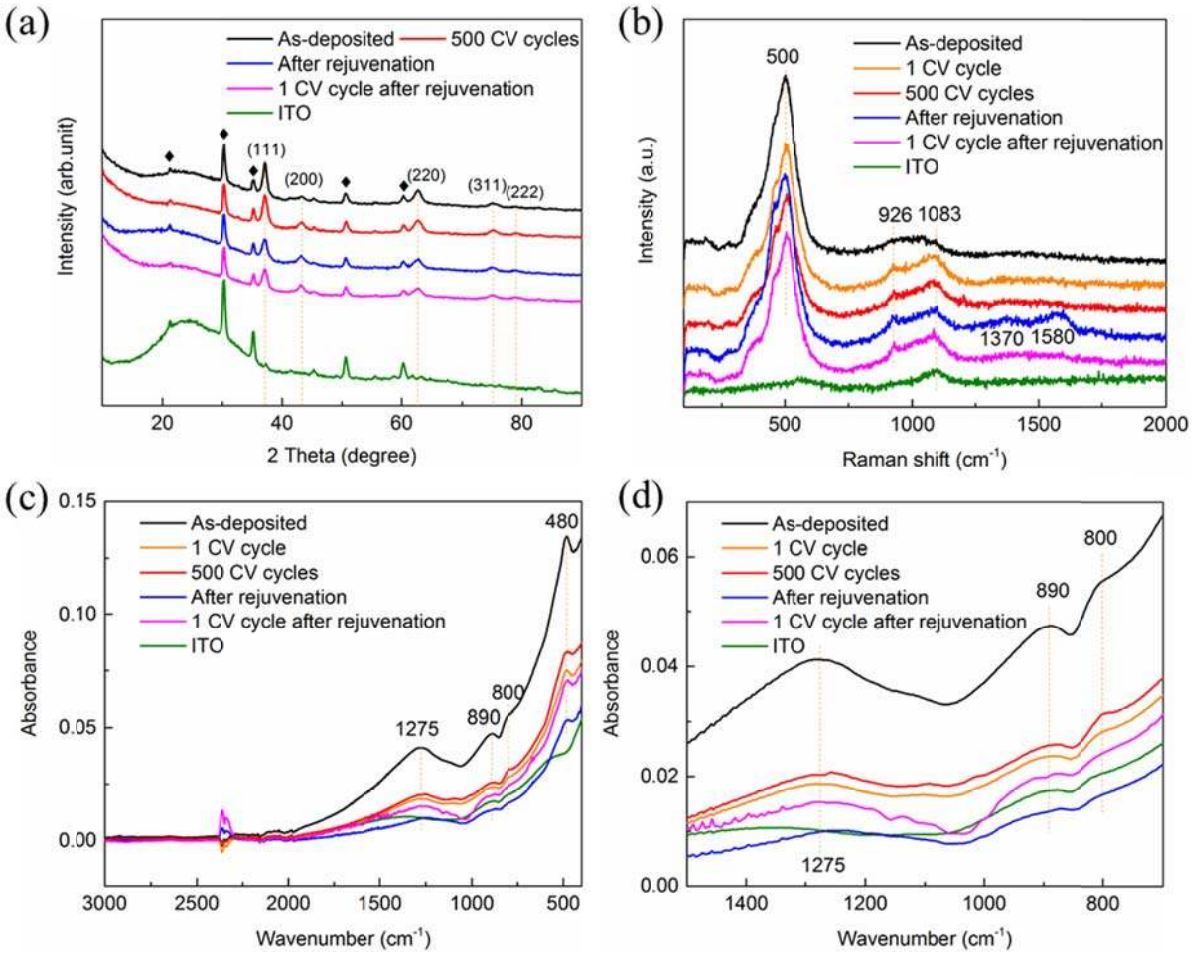

Figure 3. Structural data for a ~300-nm-thick Ni-oxide film backed by ITO and subjected to varied electrochemical operations (with CV denoting cyclic voltammetry); results are shown for as-deposited, degraded and rejuvenated samples as well as for bare ITO. (a) Vertically displaced X-ray diffractograms; vertical lines indicate the shown reflection planes in fcc NiO, and diamond-symbols refer to ITO. (b) Vertically displaced Raman spectra; vertical lines indicate peaks due to NiO at the shown wavenumbers. (c) Wide-spectrum ATR-FTIR spectra, and (d) spectra confined to the 1500–1700 cm^{-1} wavenumber range; vertical lines indicate absorbance peaks.

Vibrational spectroscopy was employed to acquire complementary structural information, and Figure 3b reports Raman data. All five recorded spectra for the Ni-oxide-based films exhibit a prominent peak at a wavenumber of about 500 cm^{-1}, corresponding to one-phonon (1P) scattering in fcc NiO,[39] which after several CV cycles and rejuvenation exhibits shoulders that can associated with hydroxide bands.[40] After CV cycling, the Ni-oxide-based film displayed peaks in the Raman spectra at 926 and 1083 cm^{-1} which can be attributed to two-phonon (2P) scattering.[41] The spectrum taken immediatly after rejuvenation shows new peaks at 1370 and 1580 cm^{-1}; they can be associated with the D and G peaks of a carbonaceous deposit on the NiO surface,[42] which probably formed during rejuvenation. However, Ni-oxide-based films that had undergone one CV cycle after rejuvenation exhibited Raman spectra that were very similar to the one just after the initial CV cycle. The Raman spectrum pertinent to ITO indicated nothing but low-intensity peaks at 570 and 1083 cm^{-1}, with the latter feature overlapping with 2P scattering in NiO.

Analogous data taken by Attenuated Total Reflectance Fourier Transform Infrared (ATR-FTIR) spectroscopy are reported in Figure 3c and, in more detail, in Figure 3d. All of the Ni-oxide-based films display rising absorbance at low wavenumbers, close to the Reststrahlen band of NiO at 465 cm^{-1}, due to the increasing extinction coefficient which couples to the evanescent IR field.[43] The absorption peak at 480 cm^{-1} is attributed to the Ni–O mode due to the surface coupled TO mode in nanostructured NiO.[44] This mode was not observed on pure ITO and is therefore not due to In–O.[45] The broad spectral features around 800 and 890 cm^{-1} are typical for librational lattice modes of OH and indicate the presence of hydroxide, in agreement with the Raman data.[46] The broad feature at 1275 cm^{-1} is due to the C–O stretch from adventitious background adsorption and is gradually decreasing as a function of CV cycling and rejuvenation. It is striking that the absorption is significantly higher in the as-deposited Ni oxide film than for the samples subjected to degradation and rejuvenation. In particular, the rejuvenated film shows a much lower absorbance than the as-prepared film. Together with the Raman spectra, which show the presence of carbon-based deposits, the data are consistent with an increased reflectivity due to formation of a carbon-containing solid/electrolyte interfacial layer. Neither Raman spectra nor ATR-FTIR data showed any evidence for vibrational modes that could be assigned to bonds with Li. Furthermore, there are no obvious differences of the film morphology upon degradation and rejuvenation.[38]

2.3 Data from Time-of-Flight Elastic Recoil Detection Analysis

The characterization data shown above do not provide information on the species involved in the electrochemical processes underlying the electrochromism of the Ni-oxide-based films or in their degradation and rejuvenation, and therefore the investigation was extended to encompass Time-of-Flight Elastic Recoil Detection Analysis (ToF-ERDA). Time-of-flight/energy coincidence recoil spectra, recorded for Ni-oxide-based films on ITO irradiated by 36 MeV I^{8+} primary ions and subjected to various treatments, are reported in Figure 4 and provide the basis for the discussion below. Clear evidence was recorded for Li, O, Cl and Ni, and trace amounts were found for H and C; in addition, Na, Si, Ca and In were observed and are believed to ensue from the ITO-coated glass substrate.[38] The ToF-ERDA data show that C concentrations of the degraded film and the rejuvenated film are 1.85 and 2.12, respectively, which means that the C concentration of the film increased 14.6% after rejuvenation. This could be an indication for the incorporation of some carbon-based deposits during the rejuvenation procedure, which is consistent with the Raman data. In the current context, the signals from Li and Cl are most interesting, and Figure 5 reports depth profiles for these species from the surface of the Ni-oxide-based film and extending to a depth of 1500×10^{15} atoms cm^{-2}, which corresponds to the full film thickness. The atomic fractions vary somewhat with depth, but average values can be deduced without difficulty and are given in Table 1 for the variously treated Ni-oxide-based films. The relative constancy of the depth profiles is likely to be due to film porosity, and one may assume that Li^+ and Cl-based ions are adsorbed at and desorbed from pore surfaces.

Table 1. Elemental concentrations of Li and Cl, and their difference, for ~300-nm-thick Ni-oxide-based films in the shown states after being subjected to varied electrochemical treatments (with CV denoting cyclic voltammetry).

Film type/treatment	Contents of Li and Cl, and their difference (at.%)		
	Li	Cl	Li – Cl
As-deposited	0	0	0
1 CV cycle (colored)	0.09	0.43	–0.34
1 CV cycle (bleached)	1.06	0.16	0.9
Degraded after 500 CV cycles	0.36	0.36	0
Rejuvenated	0.25	0.57	–0.32
1 CV cycle after rejuvenation (colored)	0.57	0.99	–0.42
1 CV cycle after rejuvenation (bleached)	0.74	0.32	0.42

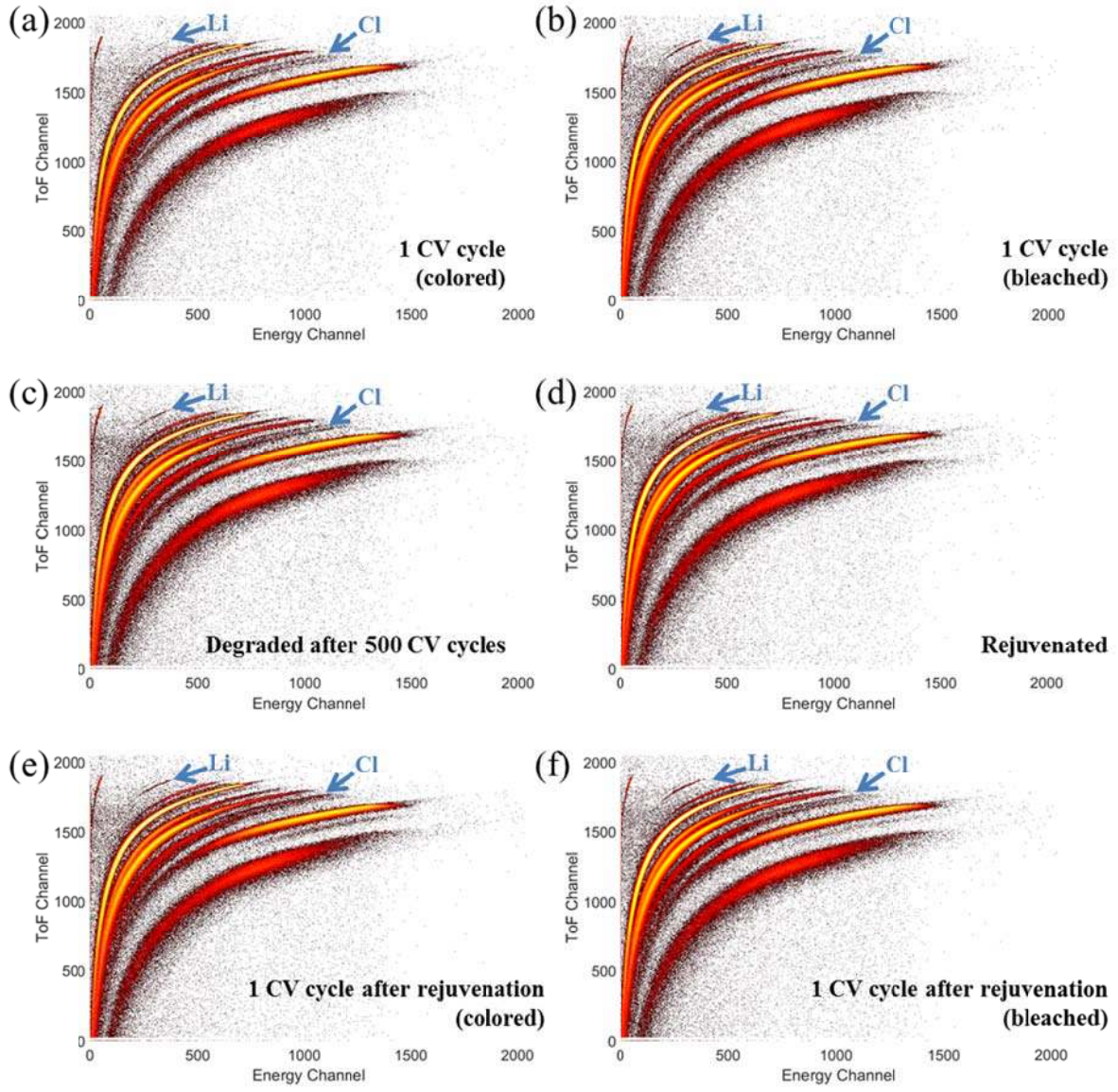

Figure 4. Time-of-flight/energy coincidence spectra of a ~300-nm-thick Ni-oxide-based film subjected to the shown electrochemical operations (with CV denoting cyclic voltammetry). Data were recorded for 36 MeV $^{127}I^{8+}$ primary ions and the elements of Li and Cl are marked.

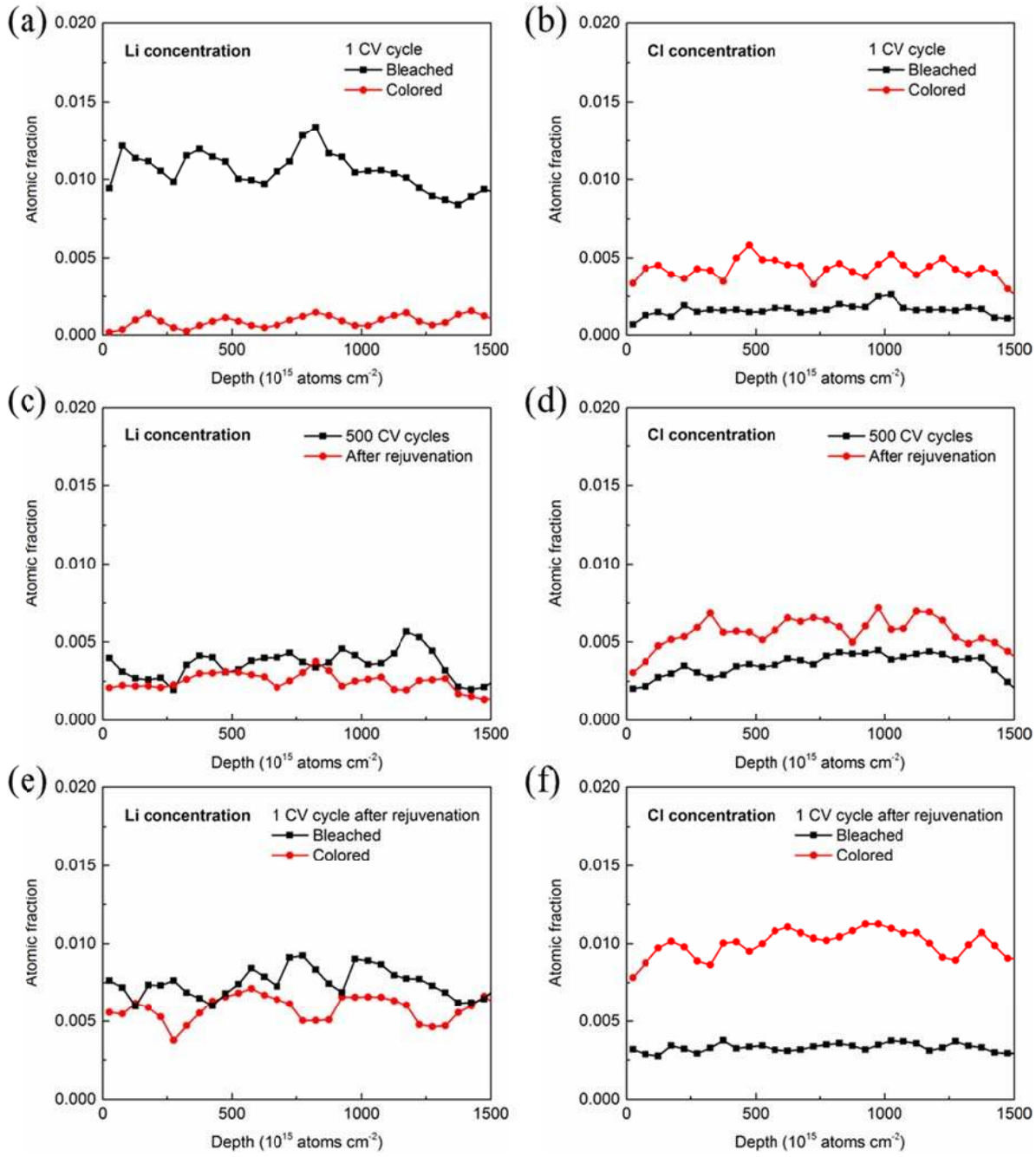

Figure 5. Depth profiles for Li and Cl as recorded by ToF-ERDA applied to a ~300-nm-thick Ni-oxide-based film immersed in $LiClO_4$–PC and subjected to the shown electrochemical operations (with CV denoting cyclic voltammetry). Data points are joined by straight lines for clarity.

Data pertaining to the first voltammetric cycle were recorded for the Ni oxide film in colored and bleached states reached at the potentials 4.0 and 2.0 V, respectively. Figures 5a, b show that the concentrations of Li and Cl vary depending on the optical properties, and the averaged Li concentration in the colored state was as small as 0.09 at.% while the Cl content

was 0.43 at.% (Table 1, second row). These concentrations may be related to Cl-based anions that were attracted to the film by electromagnetic force at 4.0 V while Li^+ ions were concurrently repelled. In the bleached state (Figures 5a, b), the Li concentration increased to 1.06 at.% while the Cl content decreased to 0.16 at.% (Table 1, third row), which may be due to reverse ionic movements at 2.0 V. These results show conclusively that the electrochromism of Ni oxide involves Li^+ cations as well as Cl-based anions: coloration occurs by extraction of cations and insertion of anions, and bleaching involves the opposite process. Furthermore, the relatively low concentrations of Li and Cl are consistent with the small charge capacity recorded during CV cycling, thus indicating that the EC processes of Ni oxide are surface-related, as suggested before.[35,36]

Elemental depth profiling of atomic concentrations was then accomplished for Ni-oxide-based films in different states: after degradation for 500 CV cycles as well as directly after rejuvenation (Figures 5c, d), and subsequent to one CV cycle after rejuvenation (Figures 5e, f). Interestingly, the degraded film had the same atomic fractions for Li and Cl, for both species being 0.36 at.% (Table 1, row 4), whereas rejuvenation decreased the Li concentration to 0.25 at.%—thus indicating removal of Li^+ ions—and raised the Cl concentration to 0.57 at.% (Table 1, row 5). It is striking that the difference in the concentrations of Li and Cl after rejuvenation (Table 1, right-hand column) became –0.32 at.%, which is almost the same as the corresponding difference during the initial CV cycle (–0.34 at.%). Considering the first CV cycle after rejuvenation, both atomic fractions increased, and the same was found for the concentration difference (Table 1, row 6). Coloring and bleaching were associated with differences in atomic fractions for Li and Cl that were analogous with those for the first CV cycle of the as-deposited Ni oxide film (Table 1, rows 6 and 7).

3. Conclusions

A comprehensive study was performed on the electrochromic properties of Ni-oxide-based films immersed in $LiClO_4$–PC with special regard to degradation upon voltammetric cycling and subsequent potentiostatic rejuvenation. Degraded films had carbonaceous surface layers, as shown from vibrational spectroscopy, whereas no changes in crystallinity were evident from X-ray diffractometry. ToF-ERDA was employed to record atomic fractions of Li and Cl over the films' cross-sections and demonstrated that exchange of *both* Li^+ anions and Cl-based cations was important for the processes underlying the electrochromism, which resolves

an issue that has been contentious until recently. Degradation was unambiguously associated with the creation of a *concentration balance* between the two ionic species, and rejuvenation was achieved by removal of Li^+ and accumulation of Cl-based ions, presumably on pore surfaces, in order to regain their initial concentration difference.

The present investigation gives guidelines towards the development of superior ion-based devices such as electrochromic glazing, but it should be observed that constructions of this kind generally incorporate more than one electrochromic thin film, which means that synergistic effects are bound to be important for practical applications.

4. Experimental Section

Ni oxide thin films were fabricated by reactive DC magnetron sputtering in a coating system based on a Balzers UTT 400 unit. The sputtering chamber contained 30 mTorr of argon and oxygen gas with an O_2/Ar ratio of 10%. Films for EC measurements were deposited onto unheated glass substrates coated with ITO having a sheet resistance of 60 Ω/sq. Substrate rotation during sputter deposition ensured film uniformity. Film thicknesses were 300 ± 10 nm as recorded by surface profilometry (Dektak XT, Bruker). More than ten samples were prepared and investigated for the various kinds of measurements.

Film crystallinity was studied by grazing incidence XRD using a Siemens D5000 diffractometer operating with CuK_α radiation at a wavelength of 1.5418 Å. Structure and phase composition were obtained by comparison with the JCPDS database.

Raman spectroscopy was performed by use of a Renishaw inVia instrument employing a frequency-doubled YAG laser (532 nm). The spectra were recorded with a 1800 lines/mm grating yielding 1-cm^{-1} resolution. All measurements were carried out using a 100× objective with 2–3 mW laser power. The optical mode of Si at 520.5 cm^{-1} from a silicon wafer was used for energy calibration. ATR-FTIR spectra were taken with a Bruker Tensor IFS 66v/S FTIR spectrometer equipped with a PIKE WeeMax III single reflection electro-ATR. The spectroscopic measurements were performed in air with 4-cm^{-1} resolution.

Cyclic voltammetry was carried out in a conventional three-electrode cell by use of a computer-controlled ECO Autolab/GPES Interface. The entire measurement was performed inside an Ar-filled glove box with a water content of about 0.5 ppm. A Ni oxide film served as working electrode and was immersed in an electrolyte of 1 M $LiClO_4$ in PC. Both counter

electrode and reference electrode were Li foils, and all voltages were measured with regard to Li/Li^+. Charge capacity C was derived from CV data by $C = \int \frac{jdV}{s}$, where j is current density, s is scan rate, and V is voltage. Spectral optical transmittance was recorded *in situ* concurrently with electrochemical cycling; data were acquired with an Ocean Optics fiber-optical instrument. The electrochemical cell was positioned between a tungsten halogen lamp and the detector, and a cell containing only the electrolyte was employed to obtain the 100-%-level for transmittance; the calibration run was performed before positioning the sample in the electrolyte.

Elemental depth profiles of the Ni-oxide-based films were established by ToF-ERDA performed at the Tandem Accelerator Laboratory of Uppsala University. Prior to measurements, the samples were washed in 1-propanol to remove electrolyte residues. Two distinct detection systems with different energy discrimination of particles after the time-of-flight drift tube, specifically using a solid-state detector and a gas detector, were used. Further technical information on the set-ups are available in the literature.[47,48]

Identification of species present in the samples was accomplished via mass discrimination and allowed unambiguous assignments up to atomic numbers of about 20; for heavier atoms, issues related to limited resolution and signal overlap associated with isotope mass distributions hampered unique identification. Absolute concentration profiles, free from references and without risks due to contributions from signals originating from different species, were calculated from the experimental time-of-flight/energy coincidence spectra by using the software CONTES.[49]

In our present work, concentrations are subject to systematic uncertainties mainly stemming from two sources: Firstly, the time-of-flight detectors are based on electron emission from ultrathin free-standing carbon foils during ion transmission, which yields detection efficiencies deviating from unity especially for light recoils. This efficiency may be as low as 40% for the case of Li—*i.e.*, for one of the most important elements in the current investigation—but the use of two separate detection systems, and the possibility to perform absolute calibration scattering with a primary beam of the species of interest from a ultra-thin film target, reduces this contribution to the systematic uncertainty to at most 15–20% of the recorded Li concentration. Much smaller uncertainties pertain to other species of concern, such as Cl. As a second contribution, the uncertainty in the specific energy loss for the primary ion in the studied material, and the specific energy loss of nuclei recoiling from the

target, give rise to additional uncertainties in the concentrations of recorded species; the maximum contribution expected from these uncertainties is on the order of 5–10% of the deduced concentration.

It should be noted, however, that both kinds of systematic uncertainties will have equivalent influences on detected concentrations of a given species in thin-film targets of similar composition. This fact implies that relative concentrations, and differences in concentrations between different samples, can be recorded independently of any influence of systematic uncertainties and are mainly governed by counting statistics in the ToF-ERDA experiments. These considerations can also account for observed scatter in the concentration profile for Li and Cl, as reported below. The corresponding uncertainties in the total resulting relative element concentrations are much smaller. From counting statistics, and due to a weak dependence of recoil cross section on atomic number, one can expect a scaling of the relative uncertainty roughly proportional to the square root of the deduced concentration, which leads to about 0.05% uncertainty for concentrations as small as 0.1% (which is relevant for Li and Cl in the present work).

Acknowledgements

Hui-Ying Qu is grateful for financial support from the China Scholarship Council Doctoral Joint-Training Program. The operation of the tandem accelerator at Uppsala University has been supported by infrastructural grants from the Swedish Foundation of Strategic Research (SSF-RIF14-0053) and the Swedish Research Council (VR-RFI-#821-2012-5144).

Conflict of Interest

The authors declare no conflict of interest.

Keywords

Electrochromism, nickel oxide film, degradation, rejuvenation, vibrational spectroscopy, ToF-ERDA

References

[1] G. B. Smith, C. G. Granqvist, *Green Nanotechnology: Solutions for Sustainability and Energy in the Built Environment*, CRC Press, Boca Raton, FL, USA, **2010**.

[2] C. G. Granqvist, *Handbook of Inorganic Electrochromic Materials*, Elsevier, Amsterdam, The Netherlands, **1995**.

[3] C. G. Granqvist, *Thin Solid Films* **2014**, *564*, 1.

[4] R. J. Mortimer, D. R. Rosseinsky, P. M. S. Monk, Eds., *Electrochromic Materials and Devices*, Wiley-VCH, Weinheim, Germany, **2015**.

[5] F. Favoino, M. Overend, Q. Jin, *Appl. Energy* **2015**, *156*, 1.

[6] P. M. Beaujuge, J. R. Reynolds, *Chem. Rev.* **2010**, *110*, 268.

[7] Y. Huang, M. Zhu, Y. Huang, Z. Pei, H. Li, Z. Wang, Q. Zue, C. Zhi, *Adv. Mater*. **2016**, *28*, 8344.

[8] G. Cai, J. Wang, P. S. Lee, *Acc. Chem. Res.* **2016**, *49*, 1469.

[9] C. G. Granqvist, M. A. Arvizu, İ. Bayrak Pehlivan, H.-Y. Qu, R.-T. Wen, G. A. Niklasson, *Electrochim. Acta* **2018**, *259*, 1170.

[10] F. Lin, D. Nordlund, T.-C. Weng, R. G. Moore, D. T. Gillaspie, A. C. Dillon, R. M. Richards, C. Engtrakul, *ACS Appl. Mater. Interfaces* **2013**, *5*, 301.

[11] Y. Lu, L. Liu, D. Mandler, P. S. Lee, *J. Mater. Chem. C* **2013**, *1*, 7380.

[12] R.-T. Wen, G. A. Niklasson, C. G. Granqvist, *ACS Appl. Mater. Interfaces* **2015**, *7*, 9319.

[13] M. A. Arvizu, G. A. Niklasson, C. G. Granqvist, *Chem. Mater*. **2017**, *29*, 2246.

[14] L. Yang, D. Ge, J. Zhao, Y. Ding, X. Kong, Y. Li, *Sol. Energy Mater. Sol. Cells* **2012**, *100*, 251.

[15] L. Liang, J. Zhang, Y. Zhou, J. Xie, X. Zhang, M. Guan, B. Pan, Y. Xie, *Sci. Rep*. **2013**, *3*, 1936.

[16] M. J. R. Scherer, U. Steiner, *Nano Lett*. **2013**, *13*, 3005.

[17] R. R. Kharade, S. S. Mali, S. S. Mohite, V. V. Kondalkar, P. S. Patil, P. N. Bhosale, *Electroanalysis* **2014**, *26*, 2388.

[18] H. Qu, X. Zhang, H. Zhang, Y. Tian, N. Li, H. Lv, S. Hou, X. Li, J. Zhao, Y. Li, *Sol. Energy Mater. Sol. Cells* **2017**, *163*, 23.

[19] R.-T. Wen, C. G. Granqvist, G. A. Niklasson, *Nat. Mater*. **2015**, *14*, 996.

[20] R.-T. Wen, G. A. Niklasson, C. G. Granqvist, *ACS Appl. Mater. Interfaces* **2015**, *7*, 28100.

[21] R.-T. Wen, M. A. Arvizu, M. Morales-Luna, C. G. Granqvist, G. A. Niklasson, *Chem. Mater*. **2016**, *28*, 4670.

[22] R.-T. Wen, G. A. Niklasson, C. G. Granqvist, *ACS Appl. Mater. Interfaces* **2016**, *8*, 5777.

[23] M. A. Arvizu, C. G. Granqvist, G. A. Niklasson, *J. Phys.: Conf. Ser*. **2016**, *764*, 012009.

[24] M. A. Arvizu, R.-T. Wen, D. Primetzhofer, J. E. Klemberg-Sapieha, L. Martinu, G. A. Niklasson, C. G. Granqvist, *ACS Appl. Mater. Interfaces* **2015**, *7*, 26387.

[25] B. Baloukas, M. A. Arvizu, R.-T. Wen, G. A. Niklasson, C. G. Granqvist, R. Vernhes, J. E. Klemberg-Sapieha, L. Martinu, *ACS Appl. Mater. Interfaces* **2017**, *9*, 16995.

[26] J. S. E. M. Svensson, C. G. Granqvist, *Appl. Phys. Lett*. **1986**, *49*, 1566.

[27] Carpenter, R. S. Conell, D. A. Corrigan, *Sol. Energy Mater*. **1987**, *16*, 333.

[28] W. Estrada, A. M. Andersson, C. G. Granqvist, *J. Appl. Phys*. **1988**, *64*, 3678.

[29] G. A. Niklasson, C. G. Granqvist, *J. Mater. Chem*. **2007**, *17*, 127.

[30] I. Bouessay, A. Rougier, P. Poizot, J. Moscovici, A. Michalowicz, J. M. Tarascon, *Electrochim. Acta* **2005**, 50, 3737.

[31] R.-T. Wen, G. A. Niklasson, C. G. Granqvist, *Thin Solid Films* **2014**, *565*, 128.

[32] R.-T. Wen, C. G. Granqvist, G. A. Niklasson, *Appl. Phys. Lett*. **2014**, *105*, 163502.

[33] R.-T. Wen, C. G. Granqvist, G. A. Niklasson, *ChemElectroChem* **2016**, *3*, 266.

[34] G. Boschloo, A. Hagfeldt, *J. Phys. Chem. B* **2001,** *105*, 3039.

[35] M. Mihelčič, A. Š. Vuk, I. Jerman, B. Orel, F. Švegl, H. Moulki, C. Faure, G. Campet, A. Rougier, *Sol. Energy Mater. Sol. Cells* **2014,** *120*, 116.

[36] R.-T. Wen, C. G. Granqvist, G. A. Niklasson, *Adv. Funct. Mater.* **2015,** *25*, 3359.

[37] G. Campet, B. Morel, M. Bourrel, J. M. Chabagno, D. Ferry, R. Garie, C. Quet, C. Geoffroy, J. J. Videau, J. Portier, C. Delmas, J. Salardenne, *Mater. Sci. Eng. B* **1991**, *8*, 303.

[38] H.-Y. Qu, D. Primetzhofer, M. A. Arvizu, Z. Qiu, U. Cindemir, C. G. Granqvist, G. A. Niklasson, *ACS Appl. Mater. Interfaces* **2017**, *9*, 42420.

[39] X. Cao, Y. Shi, W. Shi, G. Lu, X. Huang, Q. Yan, Q. Zhang, H. Zhang, *Small* **2011**, *7*, 3163.

[40] S. I. Cordoba-Torresi, A. Hugot-Le Goff, S. Joiret, *J. Electrochem. Soc*. **1991**, *138*, 1554.

[41] N. Mironova-Ulmane, A. Kuzmin, I. Steins, J. Grabis, I. Sildos, M. Pärs, *J. Phys.: Conf. Ser*. **2007**, *93*, 012039.

[42] A. C. Ferrari, J. Robertson, *Phys. Rev. B* **2000**, *61*, 14095.

[43] P. J. Gielisse, J. N. Plendl, L. C. Mansur, R. Marshall, S. S. Mitra, R. Mykolajewycz, A. Smakula, *J. Appl. Phys*. **1965**, *36*, 2446.

[44] A. J. Hunt, T. R. Steyer, D. R. Huffman, *Surf. Sci*. **1973**, *36*, 454.

[45] L. Kőrösi, S. Papp, I. Dékány, *Thin Solid Films* **2011**, *519*, 3113.

[46] A. A. Davydov, *Molecular Spectroscopy of Oxide Catalyst Surfaces*, Wiley, Hoboken, NJ, USA, **2003**.

[47] Y. Zhang, H. J. Whitlow, T. Winzell, I. F. Bubb, T. Sajavaara, K. Arstila, J. Keinonen, *Nucl. Instrum. Meth. Phys. Res. B* **1999**, *149*, 477.

[48] P. Ström, P. Petersson, M. Rubel, G. A. Possnert, *Rev. Sci. Instr.* **2016**, *87*, 103303.

[49] K. S. Janson, Internal Report, Uppsala University, Sweden, **2004**.